Plasma Sci. Technol. **25** (2023) 085502 (16pp) https://doi.org/10.1088/2058-6272/acbef4

Numerical study of the radio-frequency biased accelerating system in ion thrusters

Jinwei BAI (白进纬)[1], **Yong CAO** (曹勇)[2], **Yang LI** (李阳)[2], **Kaifa WANG** (王开发)[1], **Bin TIAN** (田滨)[2,3,*] **and Yuan HU** (胡远)[4,*]

[1] School of Science, Harbin Institute of Technology (Shenzhen), Shenzhen 518055, People's Republic of China
[2] School of Mechanical Engineering and Automation, Harbin Institute of Technology (Shenzhen), Shenzhen 518055, People's Republic of China
[3] School of Aeronautics and Astronautics, University of Electronic Science and Technology of China, Chengdu 611731, People's Republic of China
[4] State Key Laboratory of High Temperature Gas Dynamics, Institute of Mechanics, Chinese Academy of Sciences, Beijing 100190, People's Republic of China

E-mail: tianbin@hit.edu.cn and yhu@imech.ac.cn

Received 23 November 2022, revised 5 February 2023
Accepted for publication 24 February 2023
Published 28 April 2023

Abstract

A 2D-3V implicit immersed-finite-element particle-in-cell (IFE-PIC) model is introduced to investigate the radio-frequency (RF) self-bias accelerating system applied in the RF ion thruster. A set of holes in a two-grid system with slit apertures is simulated in Cartesian coordinates. The characteristics of the plasma plume, such as the ion density, the neutralization rate and the ion and electron current density were investigated for different RF voltage amplitudes (600−1200 V) and frequencies (6−30 MHz). Furthermore, the performance of the thruster was also carefully studied. The simulation results show that a well-focused plasma beam can be formed when the voltage amplitude is larger than 900 V and the frequency exceeds the reciprocal of ion transit time ($\geqslant$12 MHz) in our simulation cases. The performance of the system can be evidently improved by increasing the voltage amplitude and the frequency, and the losses of the particle and thrust are reduced correspondingly. The bulk region of the plasma beam downstream shows good quasi-neutrality, and the ions are dominant in the peripheral region when a well-focused state is achieved. The high ion density beamlet in the periphery of the ion beam is closer to the axis when the voltage amplitude is increasing, while it is expanded radially when increasing the frequency. Backstream electrons have been observed upstream, and this mainly occurs in the phase in which the electron cannot escape.

Keywords: ion thruster, radio-frequency biased grids, implicit immersed-finite-element particle-in-cell, plasma plume

(Some figures may appear in colour only in the online journal)

1. Introduction

The ion thruster, also named the gridded ion thruster (GIT), which has been gradually developed to be a mature technology since it was proposed in the 1900s [1], is extensively applied in space missions as an electric propulsion system. For instance, the NSTAR-30 ion propulsion system was used on Deep Space One [2] and Dawn [3] for the space exploration missions from NASA. Two T5 ion thrusters as the main engines were applied in the gravity field and steady-state ocean circulation explorer (GOCE) mission from ESA [4]. In addition, the microwave discharge ion engine system (μ-10) was developed for the Japanese asteroid explorer (Hayabusa) [5]. In China, the LIPS-200 ion thruster, which was designed by the Lanzhou Institute of Physics, was launched with the SJ-9 satellite in October 2012 [6].

* Author to whom any correspondence should be addressed.

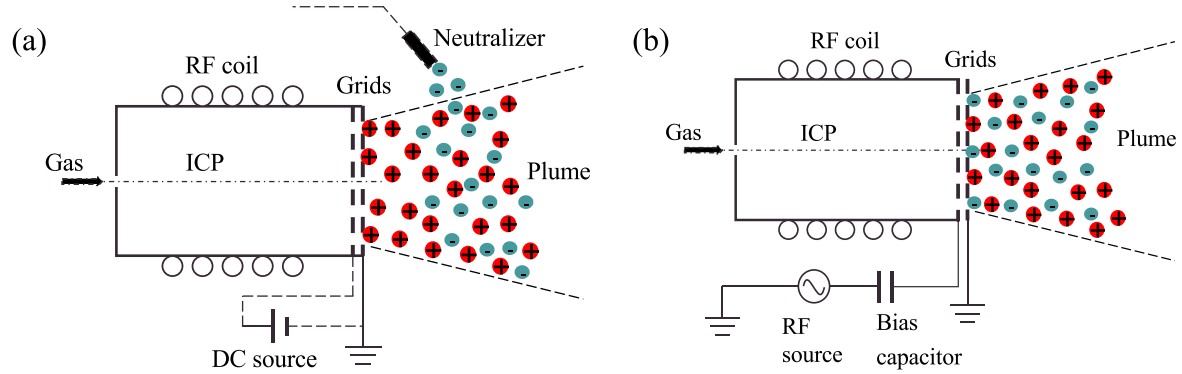

Figure 1. Schematic diagram of the GIT with (a) DC grid system and (b) RF biased grid system.

In a typical GIT, there are three stages [1, 7]: a plasma source where the plasma is generated and heated, a set of direct-current (DC) biased grids where the ion beam is extracted and accelerated, and an external neutralizer, which is applied to expel electrons and generate a quasi-neutral plume. The external neutralizer is an independent part of the main structure of the GIT; it requires an additional power supply, gas injection system and the corresponding control components [1]. The complexities of the structure are an important element constraining improvement in the performance of the GIT, although the neutralizer has been developed rapidly with the progress of materials and the design optimization.

In recent years, a novel accelerating grid system with self-neutralization, which uses radio-frequency (RF) self-bias grids instead of DC biasing, was proposed for the GIT [8–11]. In this system, the screen grid is connected to the RF source and the bias capacitor, and the accel grid is grounded. The potential drop between the screen grid and the accel grid contains a DC component and an RF component, which leads to electrons escaping intermittently and positive ions being extracted continuously [8, 11]. Therefore, the plasma beam is expected to be self-neutralized downstream, and the external neutralizer is not necessary. Figure 1 shows the comparison of the ion thrusters with the DC bias grids and the RF self-bias grids.

The first experimental prototype of the RF self-bias accelerating system, which was named 'Neptune' [8, 10], confirmed that the plasma plume could be successfully extracted and self-neutralized. The experimental results showed that the ion beam current, spatial distributions and plume properties were similar to the traditional DC acceleration. In addition, the measured ion and electron flux indicated that the ion energy distribution was multi-peaked, and the electron flux was highly anisotropic in the plasma beam region. Due to the interesting properties of two-grid RF biasing, an analytical model for predicting the self-bias voltage together with two-dimensional (2D) particle-in-cell (PIC) simulations was presented by Lafleur *et al* [12, 13] to study the electron and ion dynamics that occur as a result of RF biasing. The simulation results were consistent with previous experiments; they highlighted the dynamic motion of ions and electrons, and clarified the mechanism of ion beam space charge compensation in the downstream plume. Habl *et al* [14] also developed a 2D PIC model to study the pulsed neutralization and plasma expansion in the RF biasing system. The wave-like patterns of the ion density and the oscillation of electrons in the plume were observed in their simulations. Furthermore, the influence of different propellants on the characteristics of the plasma plume for the RF self-bias accelerating system were investigated by Li *et al* [15]. Experiments and PIC simulations were carried out in their work and it was found that a larger ion current density of Xe on the downstream surface of the accelerator grid was detected compared with that of Kr and Ar due to the larger electron density and ionization cross-section for Xe propellant. These studies for the RF self-bias system are beneficial for understanding the physical processes. However, the key parameters of this system, the amplitude of the RF voltage and the frequency, have not been fully studied. The characteristics of the plasma plume and the thruster performance varying with these two parameters have not been investigated in the literature. Therefore, the motivation of this work is to investigate the influence of the amplitude of the RF voltage and the frequency on the plasma plume and the RF accelerating grid system qualitatively and quantitatively.

In this paper, a 2D implicit immersed-finite-element particle-in-cell (IFE-PIC) model [16] is introduced to study a single set of RF grid systems. It has huge advantages in computing the plasma problems that have complex interfaces and need to be divided into regular grids [17–25]. This model can significantly reduce the computing cost [16, 26–29]. The slit structures are taken into account for the apertures of grids, and the problem is defined in Cartesian coordinates. The spatial distributions for plasma parameters, such as the ion density, the neutralization rate, the ion and the electron current density, are given to analyze the characteristics of the plasma plume. In addition, the influence of the RF voltage amplitude and the frequency on the performance of the thruster is investigated in detail. The plasma beam current density and the impingement current density to the accel grid, the divergence angle and the thrust density of the single set of grids are calculated to evaluate the performance of the system.

This paper is organized as follows. In section 2, we describe the details of the simulation model, including the calculation domain, the boundary conditions and the physical

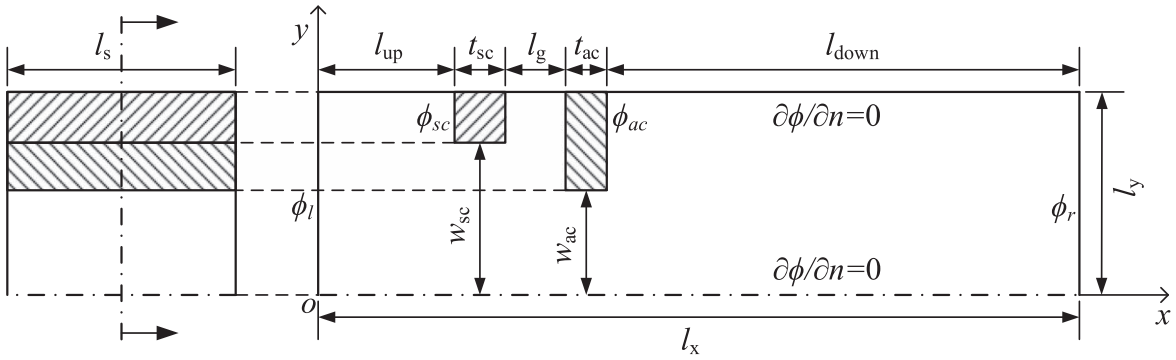

Figure 2. 2D schematic view of the simulation domain and relevant boundary conditions.

parameters. The simulation results and discussions are presented in section 3. Finally, the main conclusions are summarized in section 4.

2. Model description

2.1. Geometry of the self-bias grids

A typical two-grid RF biasing system has numerous apertures in two grids, and the accelerating plasma beam is ejected from these apertures. In order to investigate the ion optics deeply, we focus on the structure of a single set of grid apertures, which is commonly used when studying the accelerating grid system [12, 30, 31]. Figure 2 shows the geometry of the RF self-bias accelerating system for a single set of slit apertures that is also used in many studies [32–34], which is simulated in Cartesian coordinates, and the x and y coordinates refer to the axial and radial directions of the thruster.

The rectangle domain includes the accelerating grids and the plasma plume downstream. The ions and electrons that are produced in the plasma source are injected from the left-side bound. The two shaded rectangles represent the screen grid (the short one) and the accel grid (the long one), respectively. Then, the ion beam is extracted and accelerated to the downstream due to the potential drop between the grids. According to the circuit diagram shown in figure 1(b), the accel grid is grounded with the potential $\phi_{ac} = 0$ V, and the potential drop between two grids depends on the RF voltage and the DC self-bias voltage. Therefore, the potential on the screen grid is written as

$$\phi_{sc} = V_{sb} + V_{rf}\sin(\omega t) \tag{1}$$

where V_{sb} represents the self-bias voltage due to the bias capacitor, and V_{rf} is the amplitude of the RF voltage. Then, $\omega = 2\pi f$ is the angular frequency, with f the applied RF frequency. In addition, the potential at the left-side bound can be given as

$$\phi_l = V_{sheath} + V_{sb} + V_{rf}\sin(\omega t) \tag{2}$$

where V_{sheath} is the sheath potential drop in front of the screen grid. Furthermore, it is assumed that the right-side boundary in the downstream is in the far region from the grid and the potential tends to be zero, with $\phi_r = 0$ V.

Therefore, these key potentials are determined once all voltages can be given. According to the theoretical analysis by Lafleur *et al* [12, 13], the sheath potential drop near the screen grid depends on the upstream plasma and the geometry of the screen grid. We assume that the walls of the upstream plasma source are insulating and the electron and ion currents to these walls are not taken into account. Thus, the sheath potential drop is derived as [12]

$$V_{sheath} = T_e\left\{\frac{1}{2}\ln\left(\frac{m_i}{2\pi m_e}\right) - \ln\left[\frac{(1-\eta_i)A_{exit}}{A_u^s + A_h^s}\right]\right\} \tag{3}$$

where T_e is the electron temperature and the ion mass and electron mass are m_i and m_e, respectively. $A_{exit} = l_y l_s$ represents the exit area of the upstream plasma source, with l_y the length in the y direction and l_s the length of the slit aperture. η_i is the effective screen grid transparency to ions and has the relation $\eta_i A_{exit} \approx w_{sc} l_s$, and w_{sc} is the half-slit width for the screen grid. In addition, A_u^s and A_h^s are the physical areas of the upstream and grid hole barrel surfaces of the screen grid, respectively. They are expressed as

$$A_u^s = (l_y - w_{sc})l_s, \quad A_h^s = t_{sc} l_s \tag{4}$$

here, t_{sc} is the thickness of the screen grid. Similarly, the self-bias voltage can be obtained due to the current conservation on the accel grid [12]

$$V_{sb} = T_e\left\{\ln\left[I_0\left(\frac{V_{rf}}{T_e}\right)\right] - \ln\left[\frac{\gamma\eta_i(A_u^s + A_h^s)}{(1-\eta_i)(A_u^a + A_h^a)}\right]\right\} \tag{5}$$

where I_0 represents the zeroth-order modified Bessel function of the first kind and γ is the ratio of the ion current on the accel grid to the ion beam current. It is determined by the ion-neutral charge-exchange collisions [1, 12]. Moreover, the area parameters A_u^a and A_h^a have the same definitions as A_u^s and A_h^s but for the accel grid

$$A_u^a = (l_y - w_{ac})l_s, \quad A_h^a = t_{ac} l_s \tag{6}$$

where w_{ac} and t_{ac} are the half-slit width and the thickness of the accel grid, respectively. For a slit-type aperture, the length of the slit aperture l_s has no practical significance because it will be eliminated in equations (3) and (5). Once the geometry of the accelerating grids and the upstream plasma are determined, the sheath voltage and the self-bias voltage can be

calculated and the potentials mentioned above can be obtained.

2.2. The implicit PIC model

In order to investigate the RF self-bias accelerating system, a 2D-3V implicit IFE-PIC model [16] is applied to simulate the extraction and the self-neutralization of the plasma beam. The advantages of this model are applying the implicit algorithm to push the particles, and the IFE method is considered to solve the Poisson equation, which is beneficial for solving the interface problems on structured meshes efficiently and accurately [16, 17, 35].

As shown in figure 2, this simulation domain is the rectangular plane for a single set of slit-type grid apertures. Therefore, the simulations are carried out in the Cartesian coordinates. It is considered that the plasma motion is dominated by the axial and radial expansion of the plasma beam. Both electrons and xenon ions are treated as separate particles to implement a full particle simulation. The collision processes between particles are not taken into account. Thus, there is no charge exchange and energy loss between particles.

The simulation is started with no initial particles in the calculation domain. The ions and electrons are injected from the left-side boundary, satisfying the quasi-neutral condition. The initial ion velocity is considered to be the Bohm velocity, with $v_B = \sqrt{eT_e/m_i}$. Therefore, the ion current density entering the simulation domain is $j_i = en_u v_B$, with n_u the upstream plasma density. Then, the initial electron velocity is assumed to satisfy the Maxwellian distribution and the electron current density is approximately equal to $j_e = en_u \bar{v}_e$, with the electron thermal velocity $\bar{v}_e = \sqrt{8eT_e/\pi m_e}$. In addition, the particles are removed if they collide with the grids or pass through the upstream and the downstream boundaries. In the center axis and the upper boundary, the particles will be specularly reflected.

From the analysis above, the accel grid is grounded, with the potential $\phi_{ac} = 0$ V. The potential at the right downstream boundary ϕ_r is also zero due to the far region approximation. In addition, the potential drop of the upstream sheath plasma V_{sheath} and the self-bias potential drop V_{sb} can be calculated using equations (3) and (5) when the geometry of the grids and the upstream plasma are determined. Table 1 gives all parameters applied in the simulations. In our cases, the upstream sheath potential drop V_{sheath} is a constant and approximately equal to 31.8 V. Due to the relation $T_e \ll V_{rf}$, the self-bias potential drop V_{sb} is considered to be equal to the RF voltage, with $V_{sb} \approx V_{rf}$ [12]. Therefore, the potential at the screen grid ϕ_{sc} and the potential at the left boundary ϕ_l are obtained by equations (1) and (2), respectively.

Furthermore, the traditional stability conditions of the PIC simulations require the temporal step $\Delta t < 0.2/\omega_{pe}$, with ω_{pe} the electron plasma frequency and the spatial step $\Delta h < \lambda_{De}$, with λ_{De} the Debye length. However, the implicit IFE-PIC model will not be limited by these conditions. One of the advantages of this model is that the accuracy of the calculation will not be affected, even though a larger temporal step or spatial step is applied. This has been confirmed and validated in [16]. Therefore, considering that the upstream plasma density is about 10^{17} m^{-3}, the temporal step we choose here is $\Delta t = 1/\omega_{pe} = 5.6054 \times 10^{-11}$ s and the spatial step is $\Delta h = \lambda_{De} = 5.2567 \times 10^{-2}$ mm. In addition, all parameters that are listed in table 1 are unchanged in all simulations unless the variation of the parameter is studied. The parameters used in this article come from an experimental prototype (shown in figure 3) that was designed by our research group.

Table 1. Simulation parameters of the relevant operating conditions and dimensions.

Parameters	Values	Units
Total length in x direction, l_x	13.46	mm
Total length in y direction, l_y	1.68	mm
The length from upstream to screen grid, l_{up}	1.4	mm
Screen grid thickness, t_{sc}	0.56	mm
Accel grid thickness, t_{ac}	0.84	mm
Intergrid distance, l_g	0.7	mm
The length from accel grid to downstream, l_{down}	9.96	mm
Half-slit width of screen grid, w_{sc}	1.4	mm
Half-slit width of accel grid, w_{ac}	0.94	mm
RF source voltage amplitudes, V_{rf}	500−1200	V
RF source frequencies, f	5−30	MHz
Injected ion current density, j_i	35.0	Am^{-2}
Ion Bohm velocity, v_B	1.9170×10^3	ms^{-1}
Initial electron temperature, T_e	5.0	eV
Initial ion temperature, T_i	0.025	eV
Spatial step size, Δh	5.2567×10^{-2}	mm
Temporal step size, Δt	5.6054×10^{-11}	s

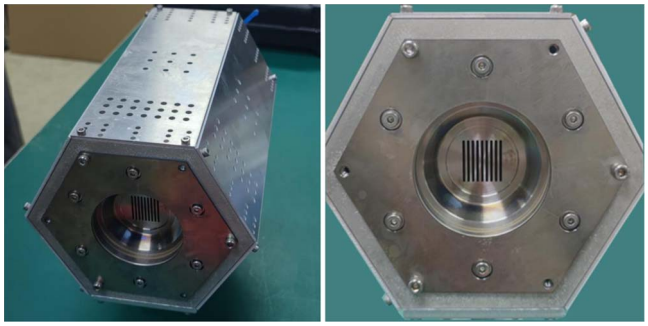

Figure 3. The experimental prototype of the RF ion thruster.

3. Results and discussions

3.1. Self-bias beam formation

In this part, the basic characteristics of the plasma beam formed by the RF self-bias grids are discussed. The amplitude of the RF voltage in this nominal simulation case is $V_{rf} = 1000$ V and the applied frequency is chosen as $f = 30$ MHz. This ensures that the ions are well focused by the electrostatic potential and the electrons escape the grid

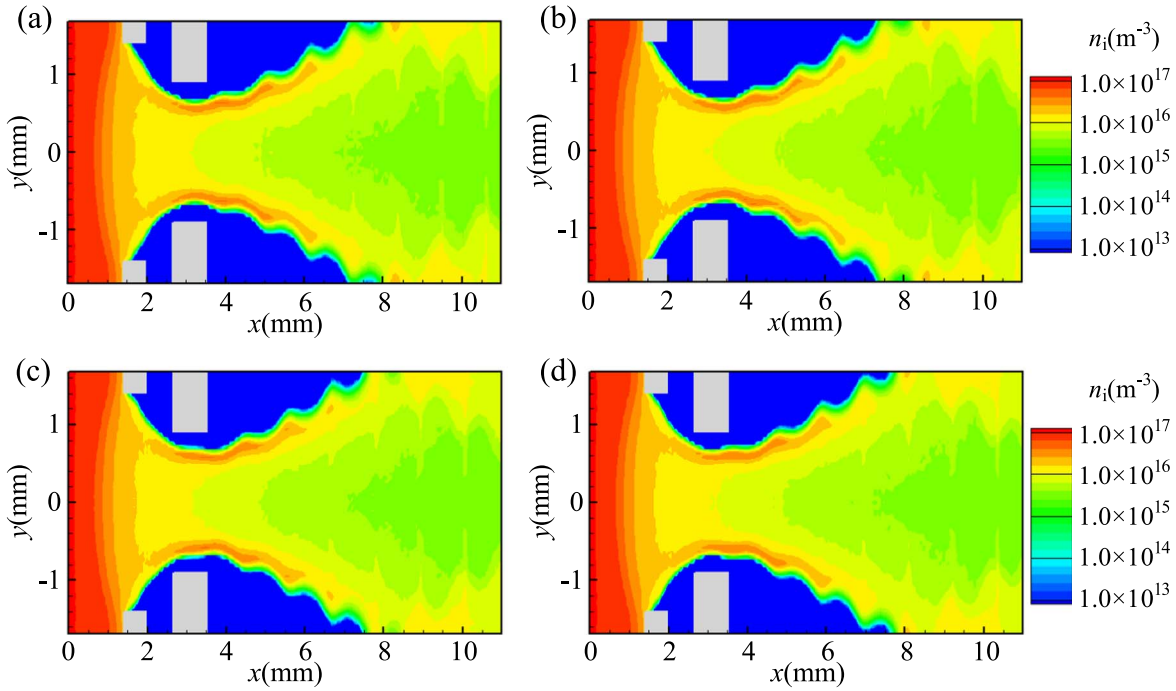

Figure 4. The 2D spatial distributions of the ion density n_i at different RF phases with (a) $\omega t = \frac{1}{2}\pi$, (b) $\omega t = \pi$, (c) $\omega t = \frac{3}{2}\pi$ and (d) $\omega t = 2\pi$. The gray rectangles denote the location of the grids. The amplitude of RF voltage is $V_{rf} = 1000$ V and the applied frequency is $f = 30$ MHz.

depending on the RF cycles. In this case, the self-bias beam reaches a quasi-steady state at $t = 5.5$ μs and all results in this paper are given after it becomes equilibrium.

We show the spatial distributions of the ion density n_i for different RF phases in figure 4. It is seen that the basic trends of the ion beam in an RF cycle are consistent. The ion density n_i has a high value in the upstream and the ions are extracted and accelerated by the self-bias girds, moving toward the downstream. The ion density becomes lower correspondingly. In addition, not only is the high density peak of the ion beam near the outer edge of the plume, but the oscillation of n_i can be observed. This phenomenon is caused by the variation of the voltage between the grids in an RF period. The periodic variation of the accelerating voltage leads to the perturbation of the plasma parameters in time, and it propagates to the downstream with the plasma plume. This result is consistent with the research in [12], which explains this phenomenon well. In addition, it is noted that the wave pattern of n_i at the outer edge has slight difference in different phases. This implies that the oscillation of the parameters can be canceled out when the averaged values in periods are obtained, and this will be confirmed later. In figure 5, the spatial distributions of the neutralization rate $(n_i - n_e)/n_i$ at different phase angles are given. Here, the effects of electrons are included. It confirms that the electrons have been strongly limited by the high electrostatic field and can only escape in a specific phase range. At $\omega t = 3\pi/2$, the accelerating voltage between the grids tends to be zero and the confinement of the electrons collapses. The electrons can easily move downstream. Therefore, it is shown that the space charge becomes more equal between the two grids, and high quasi-neutrality is observed downstream due to the diffusion of the electrons. In the center of the plasma beam, the light blue region shown in the figure represents that the electron density n_e is slightly higher than the ion density. That is because the local peak of the ion density is in the periphery of the plume and decreases gradually to the center, while the electron density is more averaged in the downstream. In the other phases, the restricted electric field for electrons is significantly high and the electrons are confined upstream. Thus, the quasi-neutral plasma can be observed upstream and the ion population dominates the space between the grids. In addition, the plasma plume shows good quasi-neutrality downstream at all RF phases. That is because all results we give here have reached the steady state. The electron has been adequately diffused downstream, though it only can escape the upstream at a specific phase range.

The spatial distributions of the ion and electron current density at different RF phases given in figures 6 and 7 show the consistency with figures 4 and 5. The oscillation of the ion current density j_i at the outer edge of the plume is clearly observed, and j_i has a relatively stable distribution at different RF phase angles. It further confirms that the ion beam can be expanded downstream in the whole RF period, and the structure of the self-bias grids can provide a stable ion beamlet as long as an appropriate RF voltage and frequency are applied. For the electron current density in figure 7, the electron beam is extensively released at $\omega t = 3\pi/2$ when the accelerating voltage between the screen and accel grid tends to be zero and no electrons can escape upstream at other RF phases. In addition, a weak backstream electron current in the center of the aperture is detected in figure 7 due to the variation in the potential drop and the reflecting of the downstream boundary. This phenomenon is very important since

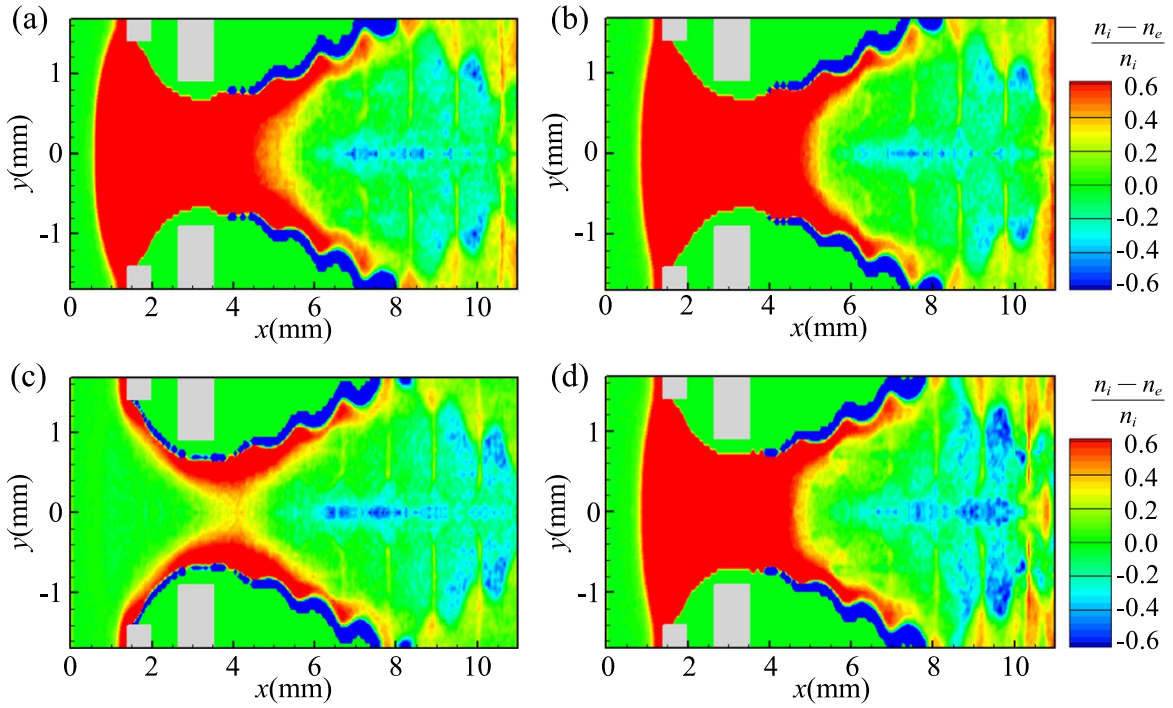

Figure 5. The 2D spatial distributions of neutralization rate $(n_i - n_e)/n_i$ at different RF phases with (a) $\omega t = \frac{1}{2}\pi$, (b) $\omega t = \pi$, (c) $\omega t = \frac{3}{2}\pi$ and (d) $\omega t = 2\pi$. The gray rectangles denote the location of the grids. The amplitude of RF voltage is $V_{rf} = 1000$ V and the applied frequency is $f = 30$ MHz.

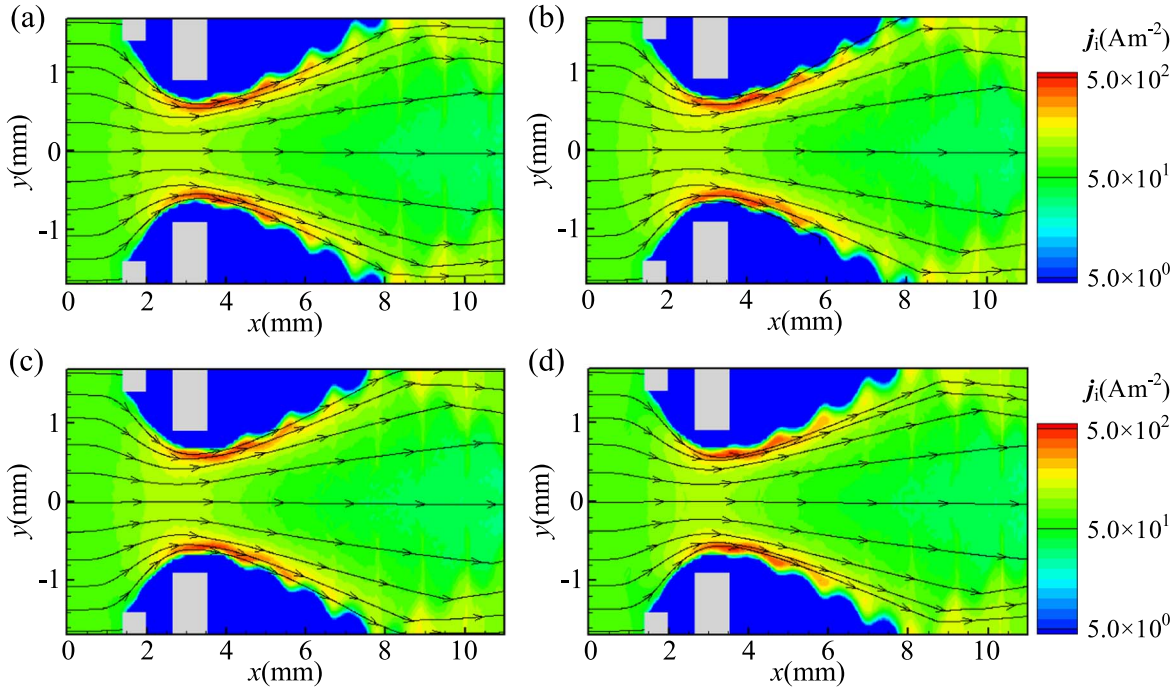

Figure 6. The 2D spatial distributions of the ion current density at different RF phases with (a) $\omega t = \frac{1}{2}\pi$, (b) $\omega t = \pi$, (c) $\omega t = \frac{3}{2}\pi$ and (d) $\omega t = 2\pi$. The solid line represents the streamline of the current density. The gray rectangles denote the location of the grids. The amplitude of RF voltage is $V_{rf} = 1000$ V and the applied frequency is $f = 30$ MHz.

the backstream electrons would compensate the current balance in RF biased systems [12].

The profiles of the potential and electric field in the axis for different RF phases and the time-averaged values are shown in figure 8. It is known that the variation of the potential upstream is mainly affected by the applied RF voltage V_{rf}. At $\omega t = \pi/2$, it has the maximum potential drop between the upstream sheath and the accel grid. The axial electric field E_x also reaches a maximum between the grids. At the phases $\omega t = \pi$ and 2π, the applied RF voltage V_{rf}

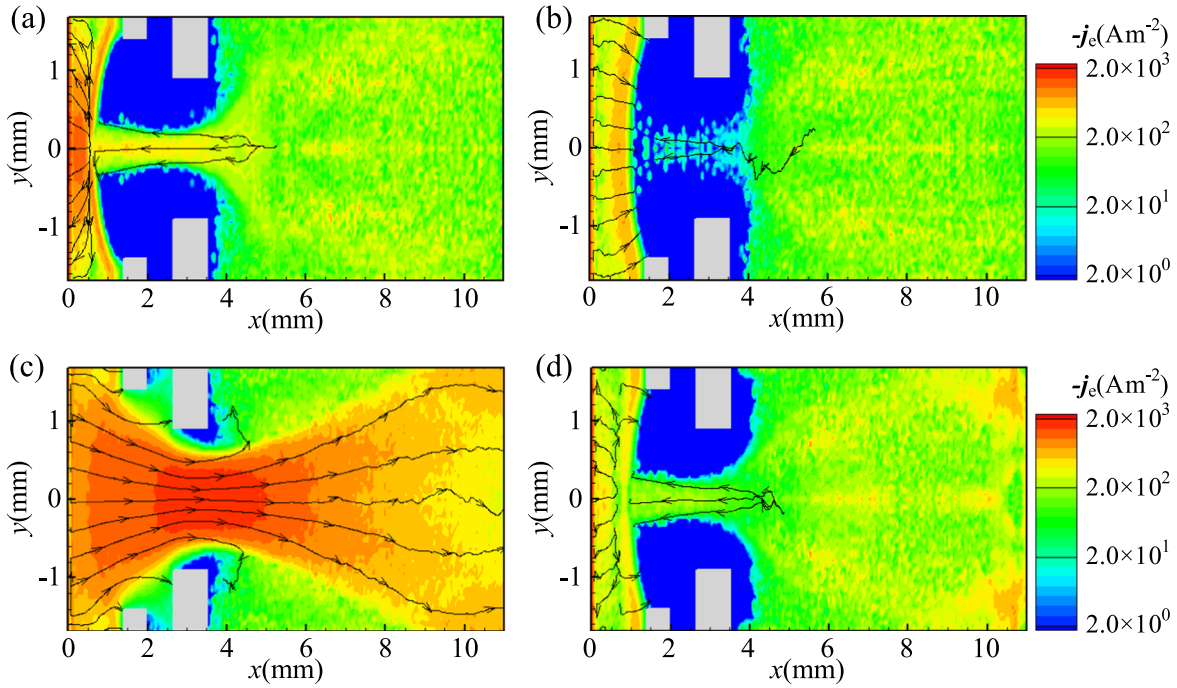

Figure 7. The 2D spatial distributions of the electron current density at different RF phases with (a) $\omega t = \frac{1}{2}\pi$, (b) $\omega t = \pi$, (c) $\omega t = \frac{3}{2}\pi$ and (d) $\omega t = 2\pi$. The solid line represents the streamline of the current density. The gray rectangles denote the location of the grids. The amplitude of RF voltage is $V_{\mathrm{rf}} = 1000$ V and the applied frequency is $f = 30$ MHz.

becomes zero and the main contribution to the potential drop is the self-bias voltage V_{sb}. In these phase ranges, the electrons are strictly confined in the upstream by the high potential barrier. However, the ions can be regularly extracted and accelerated to the downstream. At $\omega t = 3\pi/2$, V_{rf} becomes the maximum negative value, the potential drop between the upstream and the grids tends to be zero. The amount of electrons can be diffused to the downstream without the potential barrier. This behavior of the particles was confirmed in previous results. Downstream, the potential in the axis tends to be constant and the axial electric field becomes zero correspondingly, except in the region near the downstream boundary. This further implies that the downstream plasma has good quasi-neutrality, the potential in the downstream for different phases has slight difference, and the lowest potential is achieved at $\omega t = 3\pi/2$. That is because the time-varied potential drop affects the dynamic of particles. In addition, the time-averaged potential and electric field profiles in the axis are also given. The basic trend is similar to others, and this illustrates that a stable and quasi-neutral plasma plume can be formed by the RF self-bias structure in a large time scale.

Then, we show the other time-averaged plasma parameters in figure 9 in order to further understand the properties of the RF self-bias plume. The distributions of the ion density n_{i} and the ion current density j_{i} show similar trends to the results of different RF phases in figures 4 and 6. However, the oscillation of n_{i} and j_{i} in the periphery of the plume is canceled out in the time-averaged results due to the asynchronization of the wave pattern at different phases. We have mentioned this phenomenon previously, and the results verify it. For the neutralization rate, the time-averaged results clearly illustrate that the upstream and downstream plasmas have good quasi-neutrality, and the ions dominate the space of the grids. Moreover, the ion density is still much higher than the electron density in the periphery of the plume and is slightly lower in the center of the plume. In addition, the time-averaged distribution of the electron current density j_{e} is shown in figure 9(d). The main trend of the electron current is flowing to the downstream due to the main contribution of the phase $\omega t = 3\pi/2$, and it is seen that some of the electrons hit the grid. Furthermore, the electron in the upstream is trapped due to the high potential barrier and the electron in the downstream satisfies the ambipolar diffusion and is confined by the potential of the downstream boundary.

3.2. Influence of the applied RF voltage and frequency

It is known that the applied RF voltage V_{rf} and the frequency f play a significant role in the application of the RF self-bias grids. In this section, we explore the effect of these two parameters on the characteristics of the plasma plume and the performance of this self-neutralizing acceleration system. The range of voltage amplitudes $V_{\mathrm{rf}} = 600-1200$ V is investigated at a fixed frequency of $f = 30$ MHz, and the frequencies f are varied from 6–30 MHz when $V_{\mathrm{rf}} = 1000$ V.

3.2.1. Characteristics of the plasma beam. The amplitude of the applied RF voltage affects the shape of the plasma beam and the distribution of the plasma parameters, while it partially determines the power and particle loss of the system [10]. Figure 10 shows the time-averaged distributions of the ion density and the neutralization rate at different RF voltage

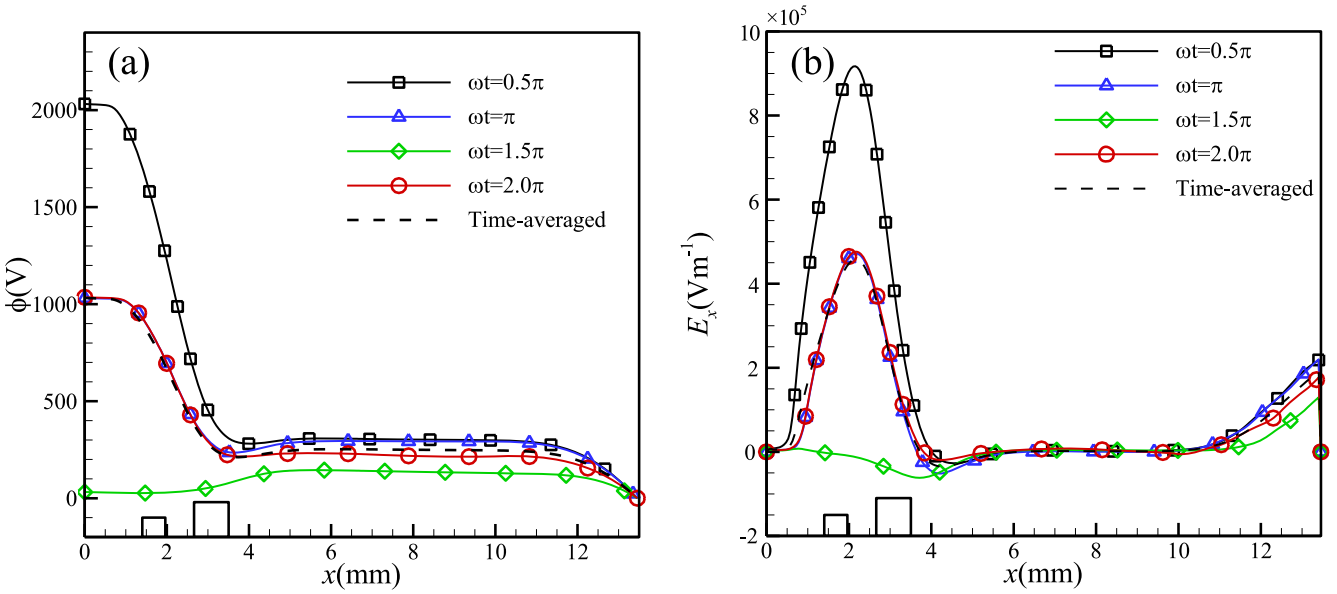

Figure 8. The profiles of (a) the potential ϕ and (b) the electric field E_x in the axis for different RF phases, and the time-averaged results. The two rectangles at the bottom denote the location of the grids. The amplitude of RF voltage is $V_{rf} = 1000$ V and the applied frequency is $f = 30$ MHz.

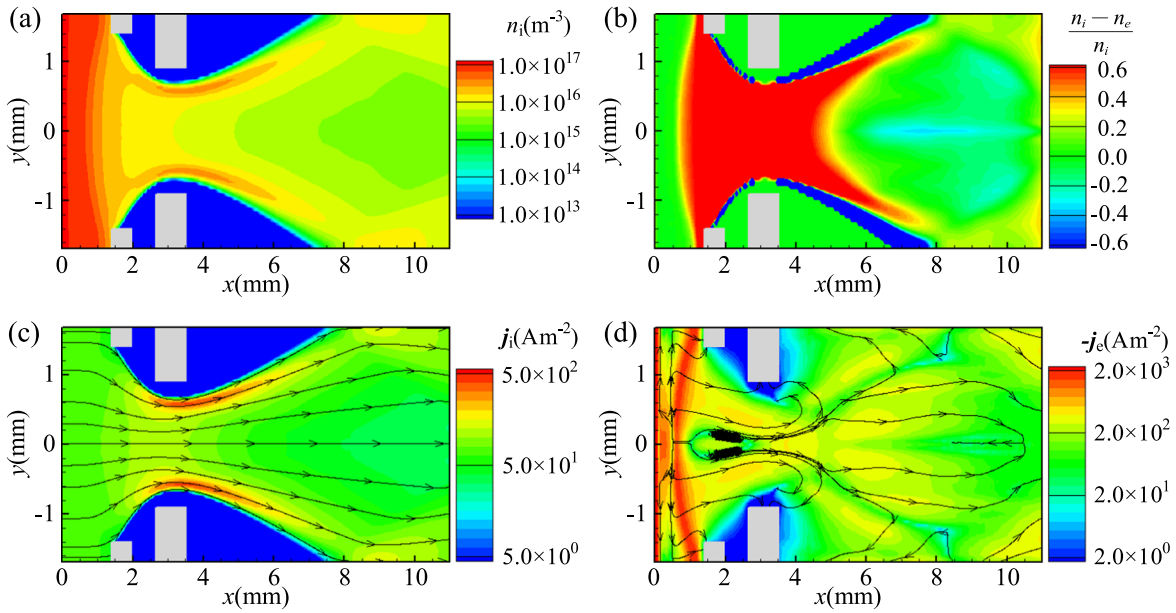

Figure 9. The 2D spatial distributions of the plasma parameters for the time-averaged (10 RF periods) results. (a)−(d) represent the ion density, the neutralization rate, the ion current density and the electron current density, respectively. The gray rectangles denote the location of the grids. The amplitude of RF voltage is $V_{rf} = 1000$ V and the applied frequency is $f = 30$ MHz.

amplitudes. As the voltage amplitude increases, the focusing of the ion beamlet is improved.

At $V_{rf} = 600$ V, the ion beam is completely under focus, and some of the ions impact the accel grid directly. The reflection of the ion beam by the lateral boundary is observed in the downstream due to the large divergence angle of the plume. When the amplitude of the voltage increases to 800 V, the ion beam has a better focus, and the crossover point of the ion beam due to the reflection moves to the far region of the downstream. As V_{rf} continues to increase, especially at $V_{rf} = 1200$ V in figure 10(c), the ion beam is well focused and the width of the beamlet is smaller than the aperture of the accel grid. Large local peaks of the ion density can be found in the periphery of the plume and there is no reflection of the ion beam by the lateral boundary in the downstream. These suggest that the ions are well confined in the center of the plume and few ions will hit the accel grid. Furthermore, the value of the amplitude of the RF voltage that can achieve a well-focused plasma beam depends on the plasma density in the upstream and the geometry of the accelerating grids, such as the width of the aperture and the distance between the screen grid and the accel grid [8].

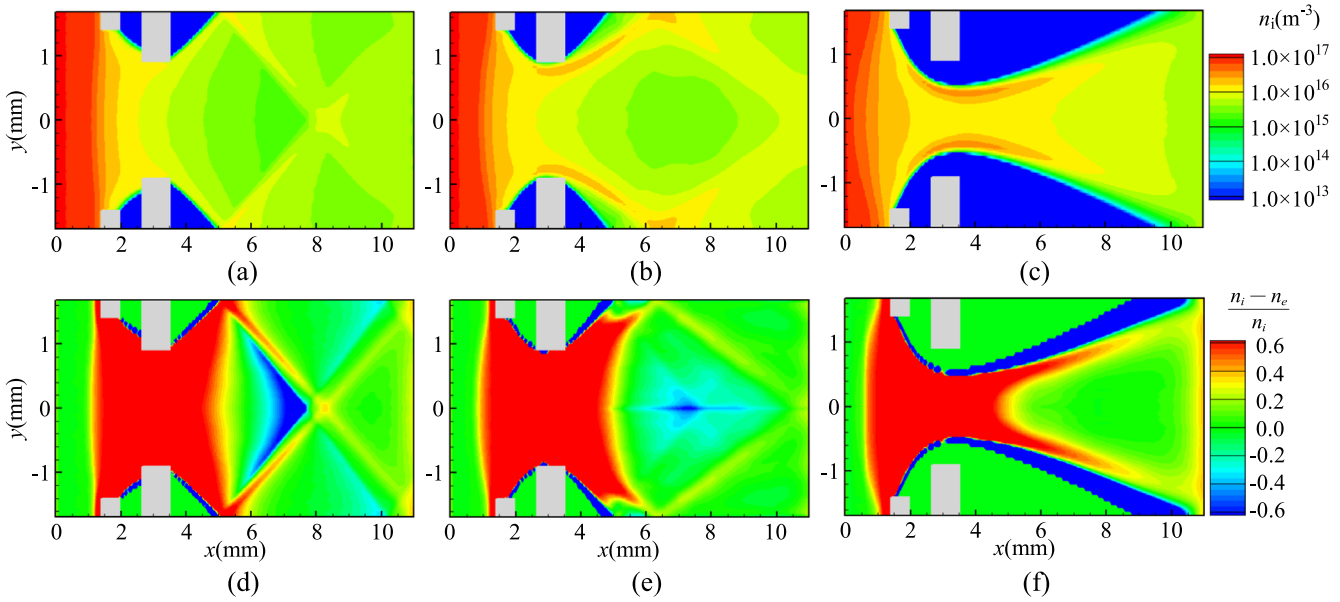

Figure 10. The time-averaged spatial distributions of the ion density and the neutralization rate for different amplitudes of the RF voltage. (a) and (d) $V_{rf} = 600$ V (left), (b) and (e) $V_{rf} = 800$ V (middle), and (c) and (f) $V_{rf} = 1200$ V (right). The gray rectangles denote the location of the grids, and the applied frequency is $f = 30$ MHz.

Then, analyzing the variation of the neutralization rate in figure 10, the ion beams are dominant in the space between the grids for all cases, and a more curved sheath edge in the upstream can be found in high-voltage cases, leading to a well-focused plasma beam. In the downstream, the bulk region of the plasma beam shows an excellent quasi-neutrality, and the ion is dominant in the peripheral region when the amplitude of the voltage V_{rf} is 1200 V. In the under-focused cases ($V_{rf} = 600$ and 800 V), the ions are diffused to a large region of the downstream and can be neutralized by the electrons, except in the region where the reflection occurs.

In order to further analyze the neutralization of the plasma plume, the radial profiles of the neutralization rate at a fixed axial position ($x = 9$ mm) for different voltage amplitudes are given in figure 11. It shows the consistency with the spatial distribution in figure 10. The quasi-neutrality is highly related to the focused state. At $V_{rf} = 1200$ V, a well-focused state is achieved and the central region of the plume has good quasi-neutrality. The maximum charge unbalance occurs in the periphery of the plume. When the voltage amplitudes decreases, the focused state changes and the quasi-neutrality becomes worse. More electrons than ions are extracted, which leads to a charge unbalance, and a negative neutralization rate is observed in the central region ($V_{rf} = 800$ V). When the ion beam is completely under-focused ($V_{rf} = 600$ V), the reflection causes a positive neutralization rate in the center.

The distributions of the current density shown in figure 12 further confirm that increasing the amplitude of the RF voltage can improve the focusing state of the plasma beam. When $V_{rf} = 600$ and 800 V, the ion beam is under-focused. The streamlines of the ion current density are more curved. At $V_{rf} = 1000$ and 1200 V (figures 9 and 12), the ions are well focused in a beamlet and expand to the downstream gradually

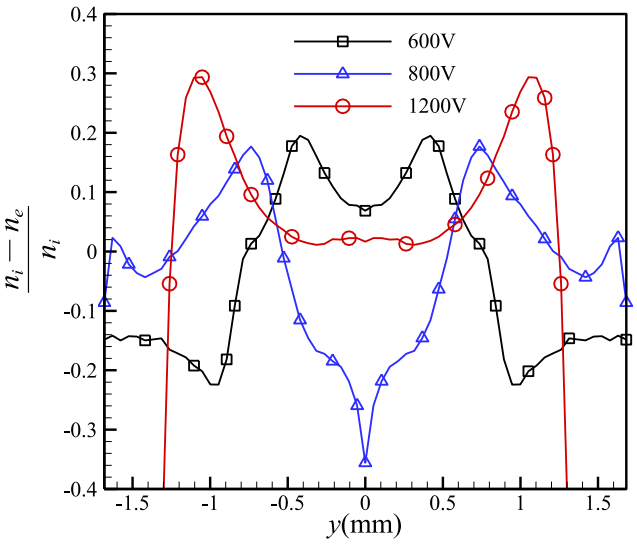

Figure 11. The radial profiles of $(n_i - n_e)/n_i$ at $x = 9$ mm for different RF voltages. The applied frequency is $f = 30$ MHz.

with a very small divergence angle. In addition, the electron current density in the bulk region of the plume is noticeably higher than in under-focused cases due to the concentration of the ions.

Next, the influence of the RF frequency on the plasma beam is investigated. It is known that the RF frequency for the self-bias accelerating system is related to the ion transit time passing through the grids and affects the focusing state [12]. If the RF frequency is too low, the ion transit time could be much smaller than the period of the RF system. The maximum ion current density, which is reached at a low accelerating voltage, will be limited according to the Child–Langmuir law [36].

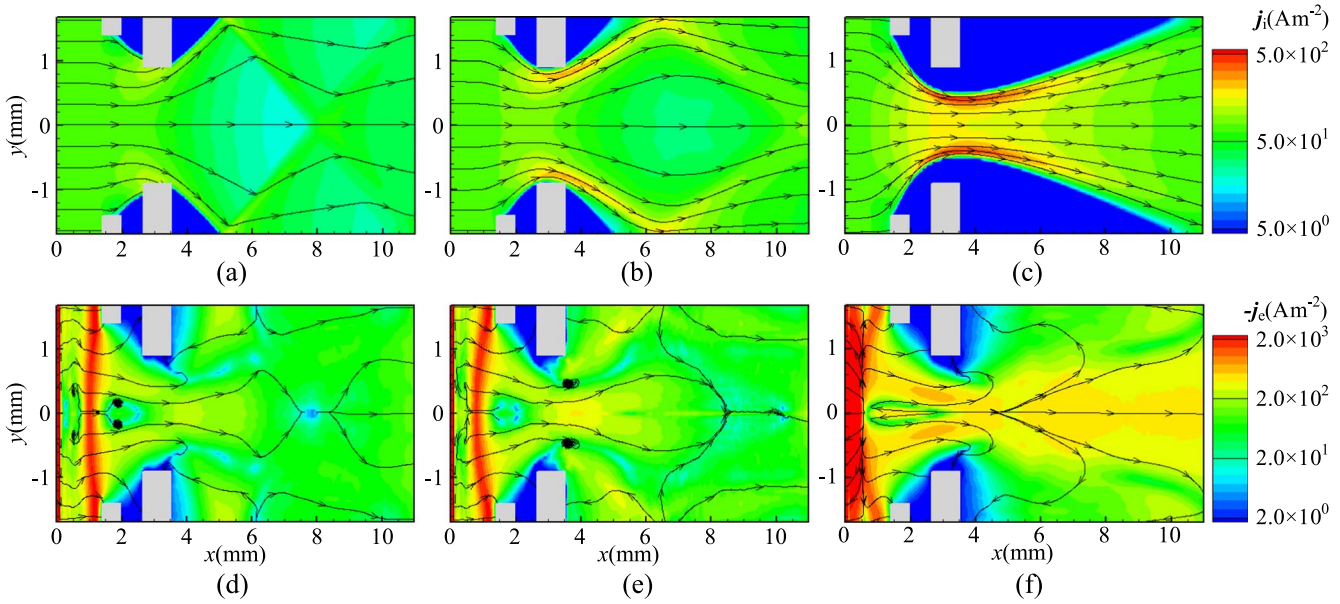

Figure 12. The time-averaged spatial distributions of the ion and electron current density for different amplitudes of the RF voltage. (a) and (d) $V_{rf} = 600$ V (left), (b) and (e) $V_{rf} = 800$ V (middle), and (c) and (f) $V_{rf} = 1200$ V (right). The gray rectangles denote the location of the grids, and the applied frequency is $f = 30$ MHz.

Figures 13 and 14 give the spatial distributions of the plasma parameters for different RF frequencies. It is concluded that a higher RF frequency is indeed beneficial to improve the focusing state if the amplitude of the voltage is large enough. At $V_{rf} = 1000$ V, the under-focused plasma beam is gradually transformed to a well-focused state by increasing the RF frequency from 6 to 20 MHz, as shown in figures 13 and 14. The number of ions colliding with the accel grid is seen to significantly diminish, and the divergence angle of the plasma beam becomes smaller at a high frequency. However, it is important to note that the effects of the RF frequency depend on the amplitude of the RF voltage. For the case of $V_{rf} = 1000$ V, the potential drop between the grids is large enough to form the focusing state. We can clearly observe the focusing ion beamlet in the aperture expanding to the downstream even if a low frequency is applied. But, when $V_{rf} = 600$ V, as shown in figures 10 and 12, the accelerating voltage is too small to form the focusing state, although the RF frequency reaches 30 MHz. Therefore, the effect of the RF frequency is to ensure that numerous ions can rapidly pass through the accelerating grid and reduce the particle loss between the grids.

Figure 15 shows the radial profiles of $(n_i - n_e)/n_i$ at $x = 9$ mm for different RF frequencies. When increasing the frequency, the position of the peak value of the neutralization rate becomes large. It illustrates that the dominant ion beamlet expands widely when the frequency is growing. It keeps the consistency with the previous results in figure 13. When the frequency is 20 MHz, a negative neutralization rate is found in the central region and a better charge balance is achieved in this region at $f = 15$ MHz.

In summary, for the amplitude of the RF voltage V_{rf} and the frequency f, increasing one of these parameters is beneficial for improving the focusing state as long as the other one is large enough. The well-focused plasma beam produced by the RF self-bias accelerating system is required to provide an appropriate amplitude of the RF voltage and the frequency. The value of V_{rf} depends on the upstream plasma density and the geometry of the accelerating grids, and the frequency f is determined by the ion transit time passing through the grids. In addition, the quasi-neutrality is well maintained in the bulk region of the plasma beam, while it becomes worse in the periphery of the plasma beam due to the ions dominating. The local peaks of the ion density in the periphery are closer to the axis when V_{rf} is increasing. On the contrary, radial expansion of the peripheral peaks is observed by increasing the frequency f.

3.2.2. Performance of the RF self-bias system. The influences of the applied RF voltage and the frequency on the performance of the self-bias accelerating system are investigated in this part. The ion beam current density, the ratio of the impingement current density to the accel grid, the thrust density of the ion beam and the divergence angle of the plasma plume are calculated by varying the voltage and frequency to evaluate the performance of the system.

The time-averaged ion beam current density as a function of the applied frequency for different voltage amplitudes given in figure 16(a) is first discussed. It is shown that a higher voltage amplitude can obtain a larger ion beam current density. When increasing the frequency f, the ion beam current density j_b grows until saturation at a specific frequency is achieved. However, the case of $V_{rf} = 600$ V is

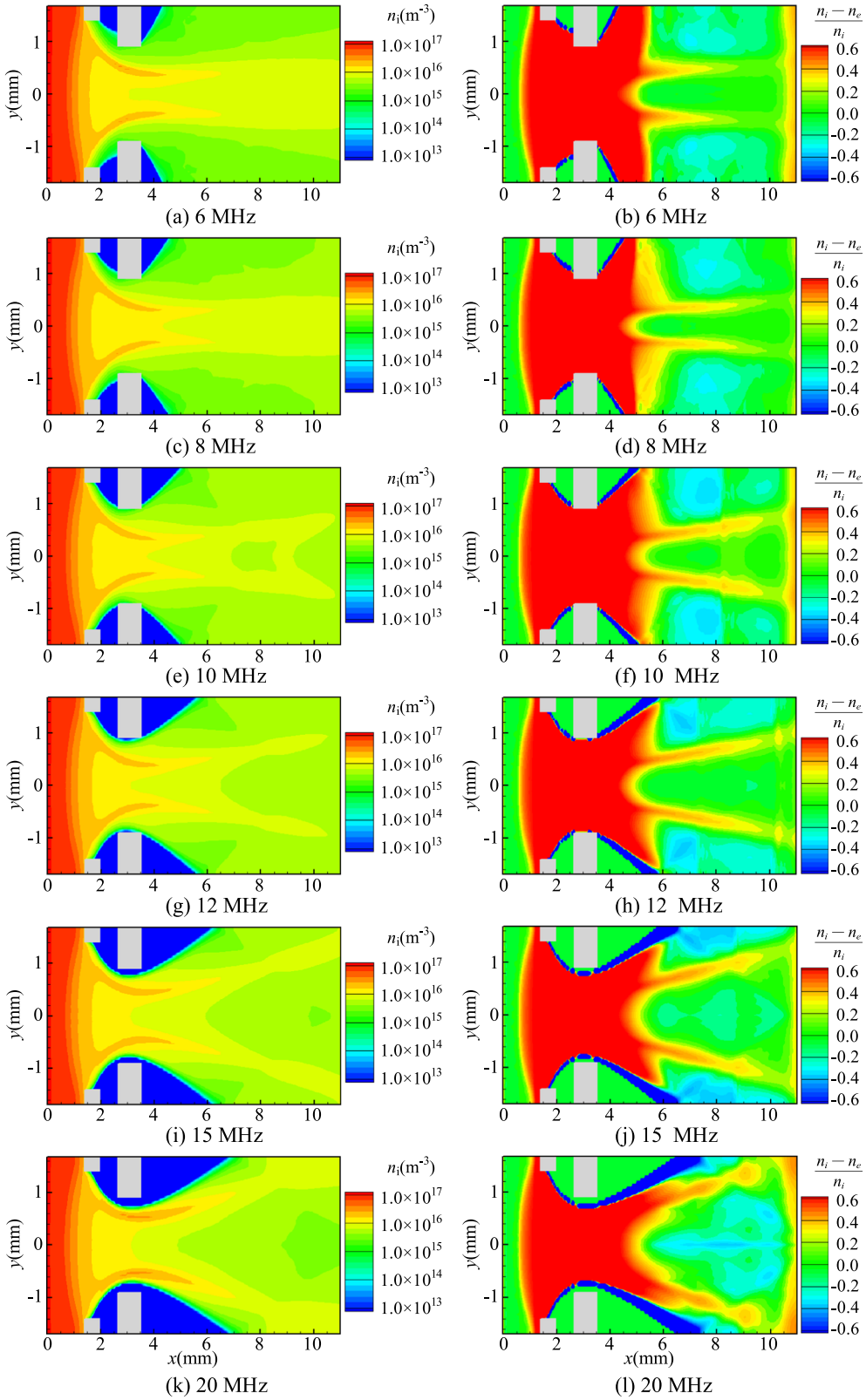

Figure 13. The time-averaged spatial distributions of the ion density and the neutralization rate for different RF frequencies. The gray rectangles denote the location of the grids, and the amplitude of the RF voltage is $V_{rf} = 1000$ V.

an exception. The ion beam current density increases in a low-frequency range and then decreases when the frequency becomes higher. That is because this voltage amplitude is too low to form the ion focusing, and numerous ions hit the accel grid directly. Increasing the frequency leads to the direct ion impingement of the accel grid more frequently, so that the ion beam current density becomes smaller. This has been confirmed by the results in figure 16(b), which will be

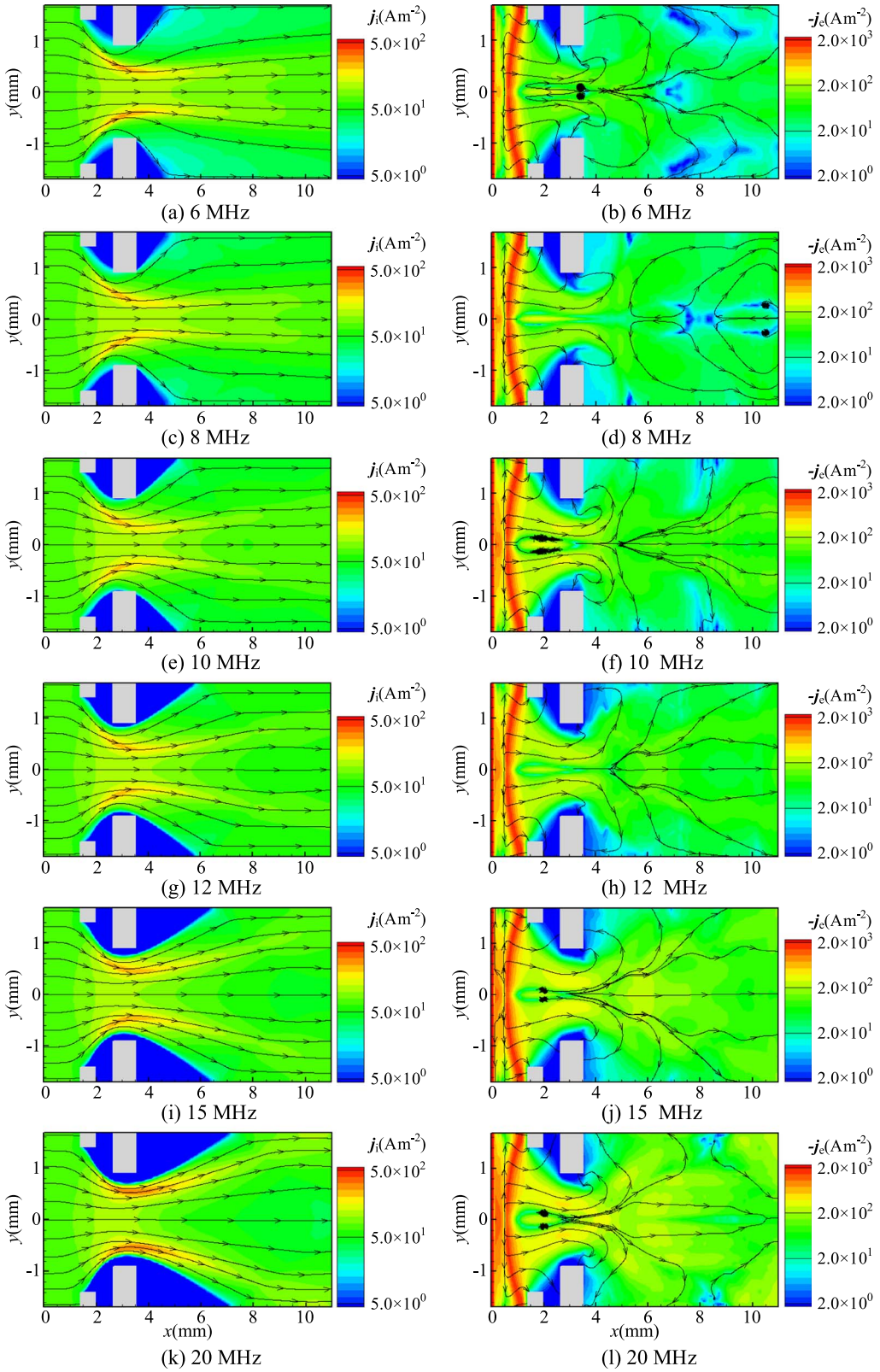

Figure 14. The time-averaged spatial distributions of the ion and electron current density for different RF frequencies. The gray rectangles denote the location of the grids, and the amplitude of the RF voltage is $V_{rf} = 1000$ V.

discussed later. Additionally, a higher V_{rf} requires a lower frequency f to achieve the saturation of the ion beam current density. At $V_{rf} = 800$ V, the ion beam current density reaches saturation when the frequency is above 20 MHz. However, the frequency decreases to 12 MHz when the voltage amplitude is 1000 and 1200 V. Therefore, the maximum ion beam current density for all cases is $j_b = 66.161$ A m^{-2} at $V_{rf} = 1200$ V and $f \geqslant 12$ MHz.

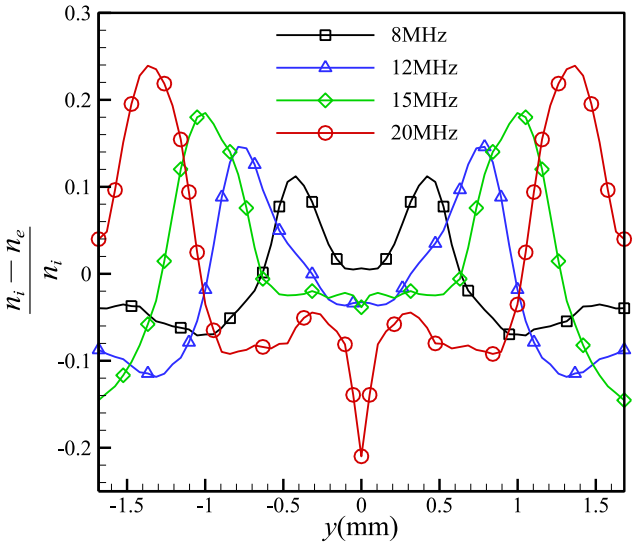

Figure 15. The radial profiles of $(n_i - n_e)/n_i$ at $x = 9$ mm for different RF frequencies. The amplitude of the RF voltage is $V_{rf} = 1000$ V.

The results of the ratio of the impingement current density on the accel grid to the ion beam current density in figure 16(b) show the consistency and further confirm the results above. At $V_{rf} = 600$ V, the impingement current density on the accel grid j_{ac} decreases in the low-frequency range and continues to increase when the frequency becomes higher due to the completely under-focused state. This suggests that the particle loss on the accel grid at $V_{rf} = 600$ is critical, and increasing the frequency will make the situation worse and lead to rapid erosion of the grid. When the voltage amplitude increases, the impingement current density j_{ac} becomes smaller and tends to zero with the increasing frequency. This is consistent with the results of figure 16(a), showing that the saturation ion beam current is achieved. Furthermore, these results can be explained by the results of figures 12 and 14. The distribution of the current density clearly shows that the RF voltage and frequency influence the focusing state largely and lead to a variation of the ion beam current density and the impingement current density. A better focusing state can improve the ion beam current density and reduce the impingement current density on the accel grid.

Then, we further study the influences of V_{rf} and f on the thrust density of the ion beam at the exit. It is an important parameter characterizing the performance of the self-bias accelerating system; in particular, the time-varying RF voltage dominates the accelerating process. The thrust density of the ion beam at the exit T_S is the ratio of thrust T to area S_e, that is $T_S = T/S_e$, and T is produced by the momentum variation and can be described as [1]

$$T = \int_{S_e} m_i n_i v_{ix} v_{ix} \mathrm{d}s \tag{7}$$

where v_{ix} represents the axial ion velocity and S_e is the section

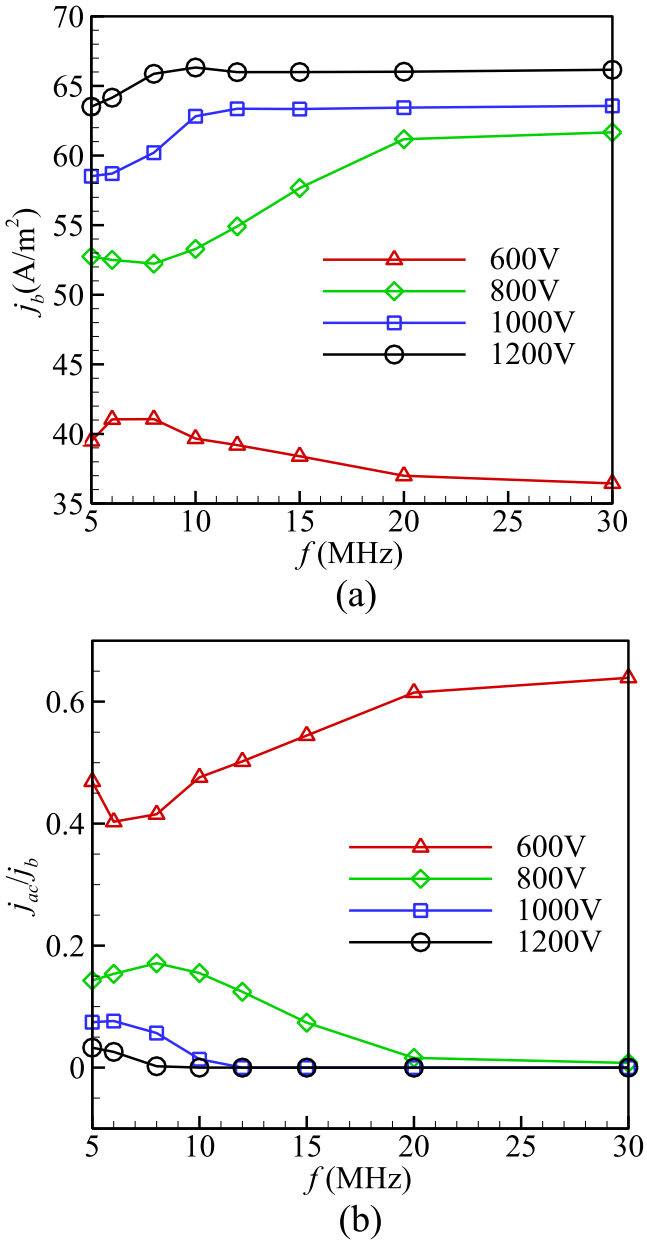

Figure 16. Time-averaged (a) ion beam current density and (b) the ratio of the impingement current density on the accel grid to the ion beam current density for different RF frequencies and voltage amplitudes.

of the accel grid exit. The thrust T is obtained by integrating the expression in the whole area of the exit section.

Figure 17 shows the time-varied thrust density of the ion beam at the exit when the voltage amplitude is $V_{rf} = 1000$ V and the frequency is $f = 30$ MHz. The evolution of the thrust density T_S in time is seen to be periodic, and the period is consistent with the RF system. This is because the accelerating process of ions is significantly affected by the RF voltage. The velocity of ions reaching the exit depends on the periodic variation of the RF voltage. Therefore, the thrust density of the ion beam naturally follows the periodic variation of the system. In addition, the thrust density T_S of the ion beam in this case is varied in the range of 7.4179–8.5791 N m^{-2}.

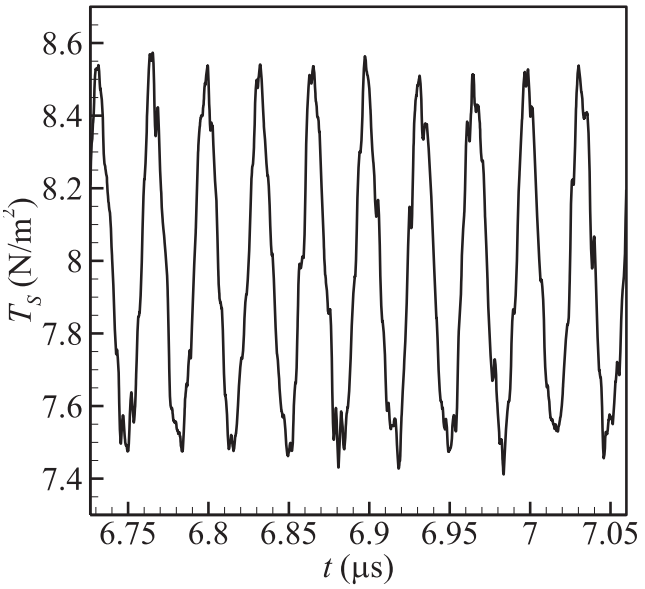

Figure 17. Time-varied thrust density of the ion beam. The amplitude of RF voltage is $V_{rf} = 1000$ V and the applied frequency is $f = 30$ MHz.

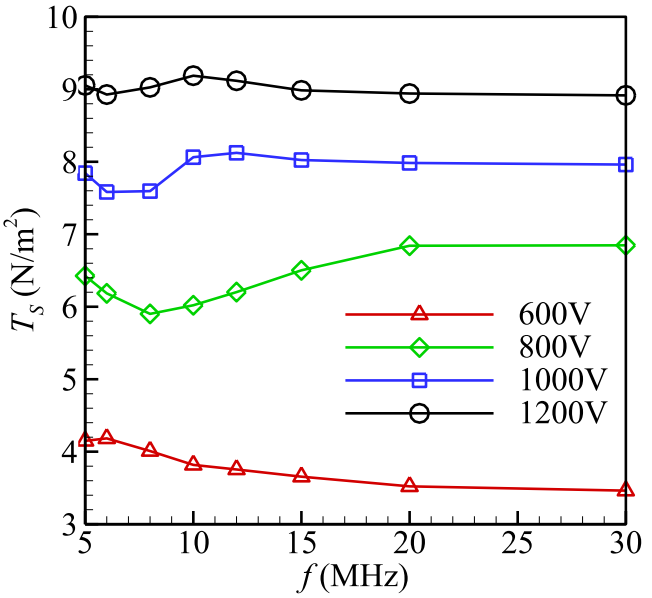

Figure 18. Time-averaged thrust density of the ion beam for different RF frequencies and voltage amplitudes.

Next, the influence of the voltage amplitude and the frequency on the thrust density T_S is discussed in figure 18. The basic trends of the thrust density show the consistency with the variation of j_b. Increasing the voltage is beneficial for improving the thrust density, and it tends to be a constant when the frequency reaches a specific value. The thrust density also depends on the focusing state of the ion beam. The well-focused plasma beam at $V_{rf} = 1200$ V and $f = 30$ MHz can produce the thrust density $T_S = 8.9163$ N m^{-2}. However, the thrust density is less than 4.5 N m^{-2} in the under-focused cases when the amplitude of the voltage is $V_{rf} = 600$ V.

Finally, the divergence angle of the ion beam varying with the amplitude of the RF voltage and the frequency is discussed here. In practice, the divergence of the plasma plume is defined as the half angle of the cone that contains 95% ion beam current [37, 38]. However, the cone is varied due to the continued radial expansion and the angle depends on the axis position. Therefore, an equivalent divergence angle α, which takes the average of the half-angle of the cone that is along the plume expansion, is applied to describe the divergence of the plasma beam.

Figure 19 gives the divergence angle α as a function of the RF frequencies for different voltage amplitudes. It is shown that, for all voltage amplitudes, the divergence of the plasma beam reduces when the RF frequency f is increasing, and the divergence angle α tends to be a constant when the frequency reaches a specific value. In the low-frequency range (less than 8 MHz), the divergence angle α varies slightly with the voltage amplitude increasing. Then, the divergence of the ion beam decreases largely beyond this frequency range. Therefore, a large amplitude of the voltage V_{rf} and frequency f can maintain the well-focused state for the ion beam and significantly limit the radial expansion of ions. The divergence which leads to the thrust loss is effectively

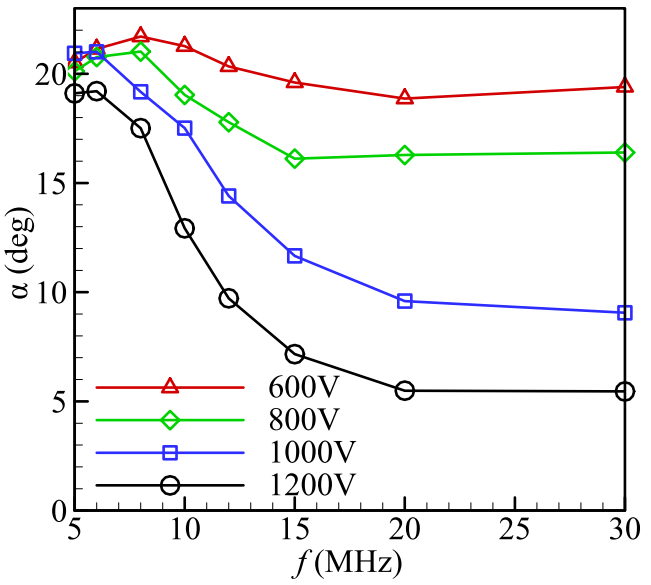

Figure 19. Time-averaged divergence angle of the plasma beam for different RF frequencies and voltage amplitudes.

reduced. For all simulation cases, the minimum divergence angle is $\alpha = 5.46°$, achieved at $V_{rf} = 1200$ V and $f = 30$ MHz.

In summary, the performance of the RF self-bias accelerating system is prominently affected by the amplitude of the RF voltage and the frequency. A large RF voltage and frequency are beneficial to improve the performance. However, it will achieve the optimum when these parameters reach a specific value, and this value for the RF voltage amplitude is determined by the upstream plasma density and the geometry of the accelerating grids; the frequency is related to the ion transit time and the voltage amplitude.

4. Conclusions

A 2D-3V implicit PIC model based on the IFE method has been applied to investigate the RF self-bias accelerating system with slit apertures. The formation of the plasma beam has been analyzed, and the influences of the amplitude of the RF voltage and the frequency on the characteristics of the plasma beam and the performance of the self-bias accelerating system have been discussed.

In our PIC simulations, a well-focused plasma beam was formed by RF self-bias grids when the voltage amplitude was larger than 900 V and the frequency exceeded the reciprocal of ion transit time ($\geqslant$12 MHz). The ion beam was extracted and accelerated in the whole RF period. However, oscillation of the ion parameters, such as the ion density and the ion current density, was observed in the periphery of the plume due to the time-varied RF voltage. The electrons escaped the upstream at a specific range of the phases, and the weak backstream electrons to the upstream were detected in the simulations. From the time-averaged results, the bulk region of the plasma beam in the downstream shows a good quasi-neutrality, and the ions are dominant in the peripheral region. In addition, the oscillation of the ion parameters found in different phases is canceled out due to the asynchronization of the wave pattern.

The RF voltage amplitude and the frequency influence the focusing state and the divergence of the ion beam. With the amplitude of the voltage or the frequency increasing, the under-focused ion beam is transformed to a well-focused state, and the divergence of the ion beam is also improved as long as the other parameter is appropriate. This process has been observed in the time-averaged distribution of the plasma parameters. In addition, it is found that the local peaks of the ion density in the periphery of the ion beam are closer to the axis when the voltage amplitude is increasing, while these high ion density beamlets are expanded radially when increasing the frequency.

Finally, the ion beam current density, the ratio of the impingement current density to the accel grid, the thrust density of the ion beam and the divergence angle of the plasma plume are analyzed when the RF voltage amplitude and the frequency are varied in order to evaluate the performance of the RF self-bias accelerating system. Increasing the voltage amplitude and the frequency can significantly improve the performance of the system, and the particle and thrust loss are reduced largely. Moreover, these two parameters have an optimal combination leading to the best performance of the system.

Acknowledgments

This work was supported by the China Postdoctoral Science Foundation (No. 2022M710977), National Natural Science Foundation of China (No. 51907039), the Natural Science Foundation of Guangdong Province (Nos. 2022A1515110215 and 2023A1515010137), and Shenzhen Technology Projects (Nos. JCYJ20190806142603534 and ZDSYS201707280904031).

References

[1] Goebel D M and Katz I 2008 *Fundamentals of Electric Propulsion: Ion and Hall Thrusters* (New York: Wiley) (https://doi.org/10.1109/AERO.2000.878373)
[2] Polk J E *et al* 2000 In-flight performance of the NSTAR ion propulsion system on the deep space one mission *IEEE Aerospace Conf. Proc.* (Piscataway, NJ: IEEE) 123
[3] Brophy J *et al* 2006 Development and testing of the dawn ion propulsion system *42nd AIAA/ASME/SAE/ASEE Joint Propulsion Conference & Exhibit* (Sacramento, CA: AIAA) 165
[4] Gollor M *et al* 2011 Electric propulsion electronics activities in Europe - 2011 *47th AIAA/ASME/SAE/ASEE Joint Prop. Con. & Exhibit* (San Diego, CA: AIAA) (https://doi.org/10.2514/6.2011-5517)
[5] Nishiyama K *et al* 2016 *Trans. Jpn. Soc. Aeronaut. Space Sci. Aerosp. Technol. Jpn.* **14** 131
[6] Liu Y W 2017 *J. Deep Space Explorat.* **4** 245 (in Chinese)
[7] Kaufman H R 1975 *Adv. Electron. Electron Phys.* **36** 265
[8] Rafalskyi D and Aanesland A 2014 *J. Phys. D Appl. Phys.* **47** 495203
[9] Rafalskyi D and Aanesland A 2014 Neutralizer-free gridded ion thruster *50th AIAA/ASME/SAE/ASEE Joint Propulsion Conf.* (Cleveland, OH: AIAA) 3423
[10] Rafalskyi D and Aanesland A 2015 *Phys. Plasmas* **22** 063502
[11] Rafalskyi D and Aanesland A 2016 *Plasma Sources Sci. Technol.* **25** 043001
[12] Lafleur T and Rafalskyi D 2018 *Plasma Sources Sci. Technol.* **27** 125004
[13] Lafleur T, Rafalskyi D and Aanesland A 2019 Radio-frequency biasing of ion thruster grids *36th International Electric Propulsion Conf.* (Vienna, Austria: IEPC) 145
[14] Habl L *et al* 2021 *Plasma Sources Sci. Technol.* **30** 045014
[15] Li Y F *et al* 2022 *Plasma Sources Sci. Technol.* **31** 035009
[16] Bai J W *et al* 2020 *Comput. Phys. Commun.* **261** 107655
[17] Lin T *et al* 2001 *Adv. Computat. Theory Pract.* **7** 107
[18] Li Z L, Lin T and Wu X H 2003 *Numer. Math.* **96** 61
[19] He X M, Lin T and Lin Y P 2008 *Numer. Methods Part. Diff. Equat.* **24** 1265
[20] He X M *et al* 2013 *Numer. Methods Part. Diff. Equat.* **29** 619
[21] Bai J W *et al* 2018 *Comput. Math. Appl.* **75** 1887
[22] Bai J W *et al* 2018 *Comput. Math. Appl.* **76** 1625
[23] Kafafy R and Wang J 2006 *IEEE Trans. Plasma Sci.* **34** 2114
[24] Kafafy R and Wang J 2007 *J. Propuls. Power* **23** 59
[25] Han D R and Wang J J 2013 Simulations of ion thruster plume contamination with a whole grid sputtered Mo source model *49th AIAA/ASME/SAE/ASEE Joint Propulsion Conf.* (San Jose, CA: AIAA) (https://doi.org/10.2514/6.2013-3888)
[26] Cohen B I, Langdon A B and Friedman A 1982 *J. Comput. Phys.* **46** 15
[27] Langdon A B, Cohen B I and Friedman A 1983 *J. Comput. Phys.* **51** 107
[28] Friedman A 1990 *J. Comput. Phys.* **90** 292
[29] Wang H Y, Jiang W and Wang Y N 2010 *Plasma Sources Sci. Technol.* **19** 045023
[30] Li H L and Sun A B 2021 *Comput. Phys. Commun.* **259** 107629
[31] Chen J J *et al* 2021 *Plasma Sci. Technol.* **23** 104002

[32] Okawa Y, Hayakawa Y and Kitamura S 2004 *Jpn. J. Appl. Phys.* **43** 1136
[33] Shagayda A and Madeev S 2016 *Rev. Sci. Instrum.* **87** 043301
[34] Melnikov A V *et al* 2022 *Acta Astronaut.* **204** 815
[35] Jian H H *et al* 2015 *Vacuum* **116** 130
[36] Lieberman M A and Lichtenberg A J 2005 *Principles of Plasma Discharges and Materials Processing, 2nd edn.* (New York: Wiley)
[37] Merino M, Cichocki F and Ahedo E 2015 *Plasma Sources Sci. Technol.* **24** 035006
[38] Sangregorio M *et al* 2018 *Chin. J. Aeronaut.* **31** 1635